Mon. Not. R. Astron. Soc. **000**, 000–000 (2013) Printed 23 January 2013 (MN LATEX style file v2.2)

Hemispherical power asymmetries in the WMAP 7-year low-resolution temperature and polarization maps

F. Paci[1⋆], A. Gruppuso[2,3], F. Finelli[2,3], A. De Rosa[2], N. Mandolesi[2,4,5], and P. Natoli[2,5,6]
[1] *SISSA - Scuola Internazionale Superiore di Studi Avanzati, via Bonomea 265, I-34136 Trieste, Italy*
[2] *INAF-IASF Bologna, Istituto di Astrofisica Spaziale e Fisica Cosmica di Bologna, via Gobetti 101, I-40129 Bologna, Italy*
[3] *INFN, Sezione di Bologna, Via Irnerio 46, I-40126 Bologna, Italy*
[4] *Agenzia Spaziale Italiana, Viale di Villa Grazioli 23, I-00198 Roma, Italy*
[5] *Dipartimento di Fisica and Sezione INFN, Università degli Studi di Ferrara, via Saragat 1, I-44100 Ferrara, Italy*
[6] *Agenzia Spaziale Italiana Science Data Center, c/o ESRIN, via Galileo Galilei, Frascati, Italy*

23 January 2013

ABSTRACT
We test the hemispherical power asymmetry of the WMAP 7-year low-resolution temperature and polarization maps. We consider two natural estimators for such an asymmetry and exploit our implementation of an optimal angular power spectrum estimator for all the six CMB spectra. By scanning the whole sky through a sample of 24 directions, we search for asymmetries in the power spectra of the two hemispheres, comparing the results with Monte Carlo simulations drawn from the WMAP 7-year best-fit model. Our analysis extends previous results to the polarization sector. The level of asymmetry on the ILC temperature map is found to be compatible with previous results, whereas no significant asymmetry on the polarized spectra is detected. Moreover, we show that our results are only weakly affected by the *a posteriori* choice of the maximum multipole considered for the analysis.

Key words: cosmic microwave background - cosmology: theory - methods: numerical - methods: statistical - cosmology: observations

1 INTRODUCTION

Since the first claim of hemispherical power asymmetry in the Cosmic Microwave Background (CMB) temperature anisotropies (Eriksen *et al.* 2004) as measured by the WMAP satellite in its first-year observation, a growing number of papers on the subject have appeared in the literature. Further investigations have refined the analysis and extended it to WMAP 3- and 5-year data (Hansen *et al.* 2004; Eriksen *et al.* 2007), leading to confirmation of a hemispherical power asymmetry - defined by Galactic coordinates $(\theta = 107^\circ, \phi = 226^\circ)$ - in the multipole range $\ell = [2, 600]$, whose significance is as high a 99.6% (Hansen *et al.* 2009).

As an alternative to a discontinuous change of the power on two opposed hemispheres, a dipolar modulation has also been considered, in the literature. In Hoftuft et al. (2009) the data resolution is lowered and a modulation of the CMB signal is assumed for angular scales up to a maximum multipole considered, $\ell_{\rm max}$. Instead, Hanson and Lewis (2009) proposed the use of an optimal quadratic estimator on full-resolution data, finding a 99.6% dipolar asymmetry on low multipoles. A critical re-analysis of the latter has been presented by the WMAP team (Bennett *et al.* 2011), where it is shown that the asymmetry is connected to the cutoff scale.

However, the polarization sector remains poorly explored in this context. Paci *et al.* (2010) investigated the properties of the CMB polarization field on the two hemispheres defined by $(\theta = 107^\circ, \phi = 226^\circ)$ (Hansen *et al.* 2009), exploiting an implementation of the quadratic maximum likelihood (QML) method (Gruppuso *et al.* 2009). No significant anomalies in the polarization and temperature-polarization cross-correlation were found in WMAP 5-year data (Paci *et al.* 2010). Dipolar modulations in temperature and polarization have been studied in Dvorkin, Peiris and Hu (2008), and more recently in Ma, Efstathiou and Challinor (2011).

In the present work we test the hemispherical power asymmetry at large scale on WMAP 7-year temperature and polarization maps without any theoretical assumptions. By sampling the whole sky in 24 equally-spaced symmetry axis, we test the power asymmetry on as many pairs of hemispheres. For each of those, we compute the same figures of merit as we did in our previous work (Paci *et al.* 2010). Moreover, we analyze the dependence of our results from the parameter ℓ_{max} along the lines suggested in Bennett *et al.*

⋆ E-mail: fpaci@sissa.it

(2011), showing that our conclusions are only mildly affected by any *a posteriori* choice.

This paper is organized as follows. In Section 2 we describe the methodology, the estimators and the dataset of our analysis. In Section 3 we present our results assessing their significance by Monte Carlo simulations. In Section 4 we draw our main conclusions.

2 DESCRIPTION OF THE ANALYSIS

In this section we review the algebra of the QML estimator, we define the 24 pairs of hemispheres under investigation and describe our dataset, simulations and estimators.

2.1 Angular Power Spectra Estimation

In order to evaluate the angular power spectra, we use the QML estimator. The QML formalism was introduced in Tegmark (1997) and extended to polarization in Tegmark and de Oliveira-Costa (2001). In this section we describe the essence of the method. Further details can be found in Gruppuso *et al.* (2009) where the *BolPol* code, our implementation of the QML estimator, has been applied to WMAP 5-year low-resolution data.

Given a map in temperature and polarization $\mathbf{x} = (\mathbf{T}, \mathbf{Q}, \mathbf{U})$, the QML provides estimates $\hat{C}_\ell^X$ - with X being one of TT, EE, TE, BB, TB, EB - of the angular power spectrum as:

$$\hat{C}_\ell^X = \sum_{\ell',X'} (F^{-1})_{\ell\ell'}^{XX'} \left[\mathbf{x}^t \mathbf{E}_{X'}^{\ell'} \mathbf{x} - tr(\mathbf{N}\mathbf{E}_{X'}^{\ell'})\right] , \quad (1)$$

where the Fisher matrix $F_{XX'}^{\ell\ell'}$ is defined as

$$F_{XX'}^{\ell\ell'} = \frac{1}{2} tr\left[\mathbf{C}^{-1} \frac{\partial \mathbf{C}}{\partial C_\ell^X} \mathbf{C}^{-1} \frac{\partial \mathbf{C}}{\partial C_{\ell'}^{X'}}\right] , \quad (2)$$

and the $\mathbf{E}_X^\ell$ matrix is given by

$$\mathbf{E}_X^\ell = \frac{1}{2} \mathbf{C}^{-1} \frac{\partial \mathbf{C}}{\partial C_\ell^X} \mathbf{C}^{-1} , \quad (3)$$

with $\mathbf{C} = \mathbf{S}(C_\ell^X) + \mathbf{N}$ being the global (signal plus noise) covariance matrix and C_ℓ^X the fiducial power spectrum.

Although an initial assumption for a fiducial power spectrum C_ℓ^X is needed, the QML method provides unbiased estimates of the power spectrum contained in the map regardless of the initial guess,

$$\langle \hat{C}_\ell^X \rangle = \bar{C}_\ell^X , \quad (4)$$

where the average is taken over the ensemble of realizations and $\bar{C}_\ell^X$ denotes the underlying model. The covariance matrix associated to the estimates is the inverse Fisher matrix,

$$\langle \Delta\hat{C}_\ell^X \Delta\hat{C}_{\ell'}^{X'} \rangle = (F^{-1})_{\ell\ell'}^{XX'} , \quad (5)$$

and it does depend on the assumption for the fiducial power spectrum C_ℓ^X: the closer the guess to the true power spectrum is, the closer are the error bars to minimum variance. According to the Cramer-Rao inequality, Eq. (5) tells us that the QML has the smallest error bars. We thus call the QML an 'optimal' estimator.

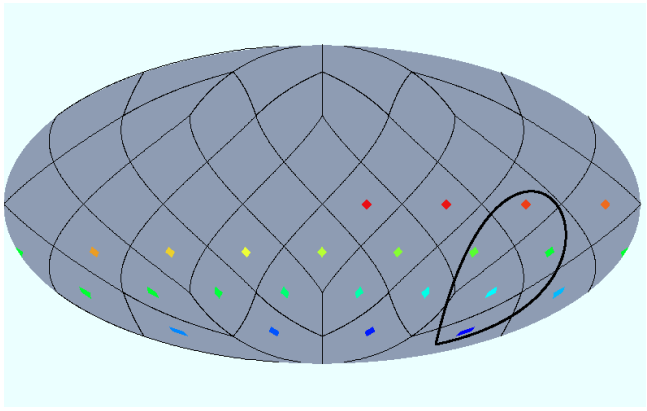

Figure 1. Mollweide projection of the 24 directions defined by Healpix resolution parameter $N_{\rm side} = 2$. Galactic coordinates of each axis are reported in Table 1, following the color scale from blue ($\hat{n}_1$) to red ($\hat{n}_{24}$). The black line defines the area of interest (see subsection 3.1).

Table 1. Galactic coordinates of the 24 directions shown in Fig. 1.

$\hat{n}$	θ (deg)	ϕ (deg)	$\hat{n}$	θ (deg)	ϕ (deg)
$\hat{n}_1$	153	225	$\hat{n}_{13}$	112	180
$\hat{n}_2$	153	315	$\hat{n}_{14}$	112	225
$\hat{n}_3$	153	45	$\hat{n}_{15}$	112	270
$\hat{n}_4$	153	135	$\hat{n}_{16}$	112	315
$\hat{n}_5$	132	200	$\hat{n}_{17}$	112	0
$\hat{n}_6$	132	245	$\hat{n}_{18}$	112	45
$\hat{n}_7$	132	290	$\hat{n}_{19}$	112	90
$\hat{n}_8$	132	335	$\hat{n}_{20}$	112	135
$\hat{n}_9$	132	25	$\hat{n}_{21}$	90	200
$\hat{n}_{10}$	132	70	$\hat{n}_{22}$	90	245
$\hat{n}_{11}$	132	115	$\hat{n}_{23}$	90	290
$\hat{n}_{12}$	132	160	$\hat{n}_{24}$	90	335

2.2 Direction sampling

In order to uniformly sample the sky, we have chosen 24 directions as shown in Fig. 1. For each of those, we have built a pair (North/South) of hemispherical masks at Healpix[1] (Gorski *et al.* 2005) resolution $N_{\rm side} = 16$. In Table 1 we report the Galactic coordinates of the directions considered. The hemispherical masks have been combined with the WMAP low-resolution Galactic masks for temperature (KQ85) and polarization (P06).

2.3 Dataset and Simulations

We use the temperature ILC map smoothed at 9.8 degrees and reconstructed at HealPix resolution $N_{\rm side} = 16$, the foreground cleaned low-resolution maps and the noise covari-

[1] http://healpix.jpl.nasa.gov/

Table 2. Probability for R and D of having a smaller value with respect to the WMAP one along direction $\hat{n}_{14}$.

$TT(\hat{n}_{14})$	$\ell = 2-16$	$\ell = 2-24$	$\ell = 2-32$
R	90.94	96.16	98.38
D	84.63	89.86	95.57

ance matrix in (Q, U) publicly available at the LAMBDA website[2]. We have added to the temperature map a random noise realization with variance of $1\mu K^2$, as suggested in Dunkley *et al.* (2009). Consistently, the noise covariance matrix for TT is taken to be diagonal with variance equal to $1\mu K^2$.

Maps and covariances for the two sky regions (namely North and South) have been consistently tailored to the combined masks.

To assess the significance of the power asymmetries found in the data, our results have been tested against Monte Carlo simulations. A set of 10000 CMB+noise sky realizations has been generated: the signal was generated from the WMAP 7-year best-fit model (Komatsu *et al.* 2011), the noise through a Cholesky decomposition of the global (T, Q, U) noise covariance matrix. We have then computed the angular power spectra for each of the 10000 simulations using *BolPol* and built two figures of merit as explained in the next subsection.

2.4 Estimators

We define the following quantities

$$C^X_{N/S} \equiv \frac{1}{(\ell_{\rm max}-1)} \sum_{\ell=2,\ell_{\rm max}} \frac{\ell(\ell+1)}{2\pi} \hat{C}^{X,N/S}_\ell \qquad (6)$$

where $\hat{C}^{X,N}_\ell$ and $\hat{C}^{X,S}_\ell$ are the estimated angular power spectra obtained with *BolPol* observing only the Northern ('N') and the Southern ('S') hemisphere respectively, outside the galactic plane. As above, X runs over the spectral types.

Two estimators can be built as follows: the ratio R^X, as performed in Eriksen *et al.* (2004),

$$R^X = \max\{C^X_S/C^X_N\,, C^X_N/C^X_S\} \qquad (7)$$

and the difference D^X,

$$D^X = |C^X_S - C^X_N|\,, \qquad (8)$$

of the two aforementioned quantities. In the following, we will drop the index X for R and D, and mention explicitly the spectrum we refer to.

For our application to WMAP data, both estimators may be considered for TT, while only the D estimator has been applied to the other spectra (EE, TE, BB, TB and EB), because of unfavorable signal-to-noise ratio of the WMAP data in polarization.

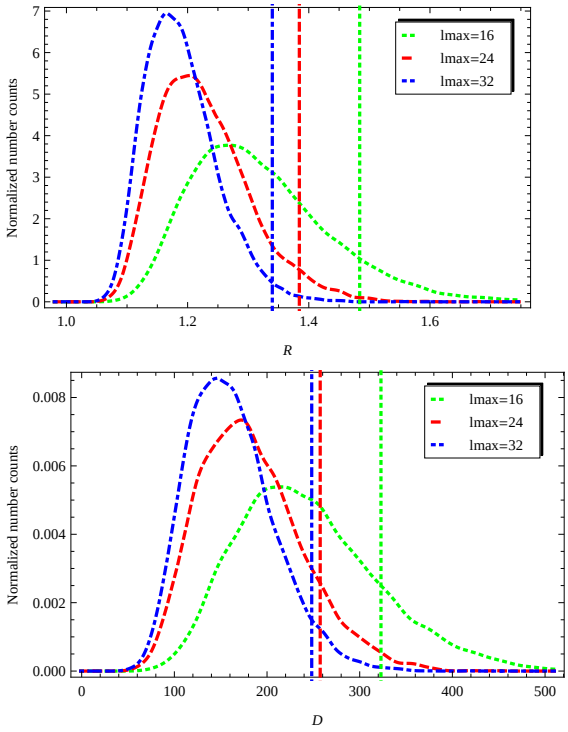

Figure 2. Top panel: estimator R for TT computed for $\ell_{\rm max} = 16$ (dotted green), 24 (dashed red), 32 (dot-dashed blue), for direction $\hat{n}_{14}$, the one closer to the axis found by Hansen *et al.* (2009). The vertical lines show the value we extract from the WMAP data whereas the smoothed probability distribution are drawn from Monte Carlo simulations. Bottom panel: same for estimator D.

3 RESULTS

As preliminar result, we report in Fig. 2 our estimate of the temperature hemispherical asymmetry defined by direction $\hat{n}_{14}$ (the one within our sample which lies closer to the axis found by Hansen *et al.* (2009)), for three values of the maximum multipole considered, taken as illustrative, $\ell_{\rm max} = 16$, 24, 36. The two panels show the value of R and D as computed for the WMAP maps, compared to the probability distributions we have drawn from Monte Carlo simulations. The corresponding level of asymmetry is explicitly shown in Table 2 for the corresponding multipole intervals. The Monte Carlo distribution does not depend on the specific direction considered, as the estimators are computed by maximizing the asymmetry over the 24 directions under investigation (see Subsection 3.2 for more details).

However, our extension of the same analysis to other direction in the sky suggests that also directions $\hat{n}_1$, $\hat{n}_6$, $\hat{n}_{15}$ and $\hat{n}_{22}$ have a comparable, or even higher, level of power asymmetry. This is shown in Fig. 3, where we plot the percentage level of hemispherical asymmetry as defined by our sample of 24 directions for the same three maximum angular scales, $\ell_{\rm max} = 16$, 24, 36. Those correspond to the region highlighted by the black circle in Fig. 1. We will further investigate such region in the next subsection.

[2] http://lambda.gsfc.nasa.gov/

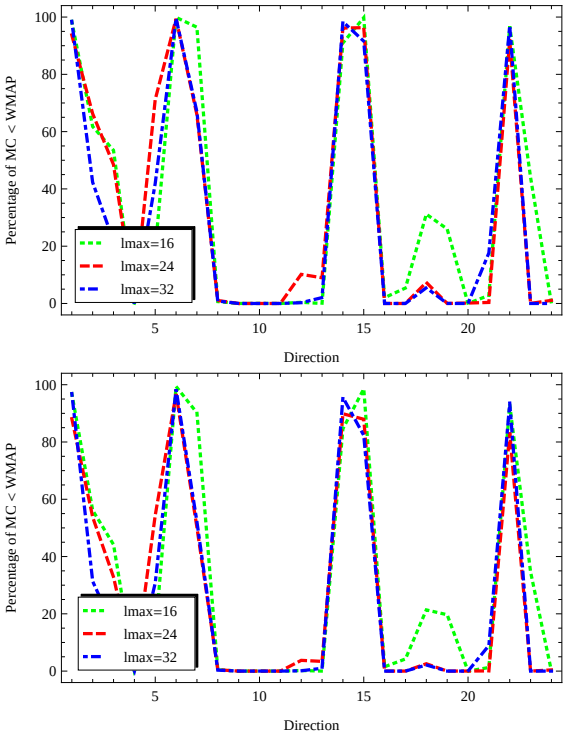

Figure 3. Top panel: percentage asymmetry of the estimator R for TT computed for $\ell_{\rm max} = 16$ (dotted green), 24 (dashed red), 32 (dot-dashed blue) along each of the 24 directions considered. Bottom panel: same for estimator D.

No significant hemispherical asymmetry is manifest in the cross- and polarization spectra (see Fig. 4), where the low signal-to-noise ratio reflects onto ℓ-dependent fluctuations of D. We have also checked that TB and EB cross-spectra are well consistent with no asymmetry.

3.1 Angular scale dependence

We focus in this section on the most anomalous directions for the temperature field and investigate their multipole dependence. We restrict to directions $\hat{n}_1$, $\hat{n}_6$, $\hat{n}_{14}$, $\hat{n}_{15}$, $\hat{n}_{22}$ and let $\ell_{\rm max}$ vary from 2 to 32. Results are reported in Figs. 5,6. We observe that the cumulative power up to multipoles $\ell \sim 8$ does not show significant asymmetry, for none of the 5 hemispherical pairs considered. The only exceptions are $\ell = 2$ and $\ell_{\rm max} = 4$ for $\hat{n}_6$ and $\hat{n}_{15}$ respectively. We also notice that direction $\hat{n}_6$ (red curve), defined by Galactic coordinates ($\theta = 132°$, $\phi = 245°$), shows a constant, very high level of asymmetry through almost all the multipoles explored here, reaching the maximum for $\ell_{\rm max} = 14$ as high as 99.99% (99.82%) for R (D).

3.2 Monte Carlo simulations

Throughout the present work, uncertainties are assessed by Monte Carlo simulations [3]. For each simulated CMB sky, the

[3] We sample our distributions by 10000 MC simulations. This introduces a resolution scale of $\sim 0.01\%$ in our assessments and prevents us from properly exploring effects at more than $\sim 3.5\sigma$.

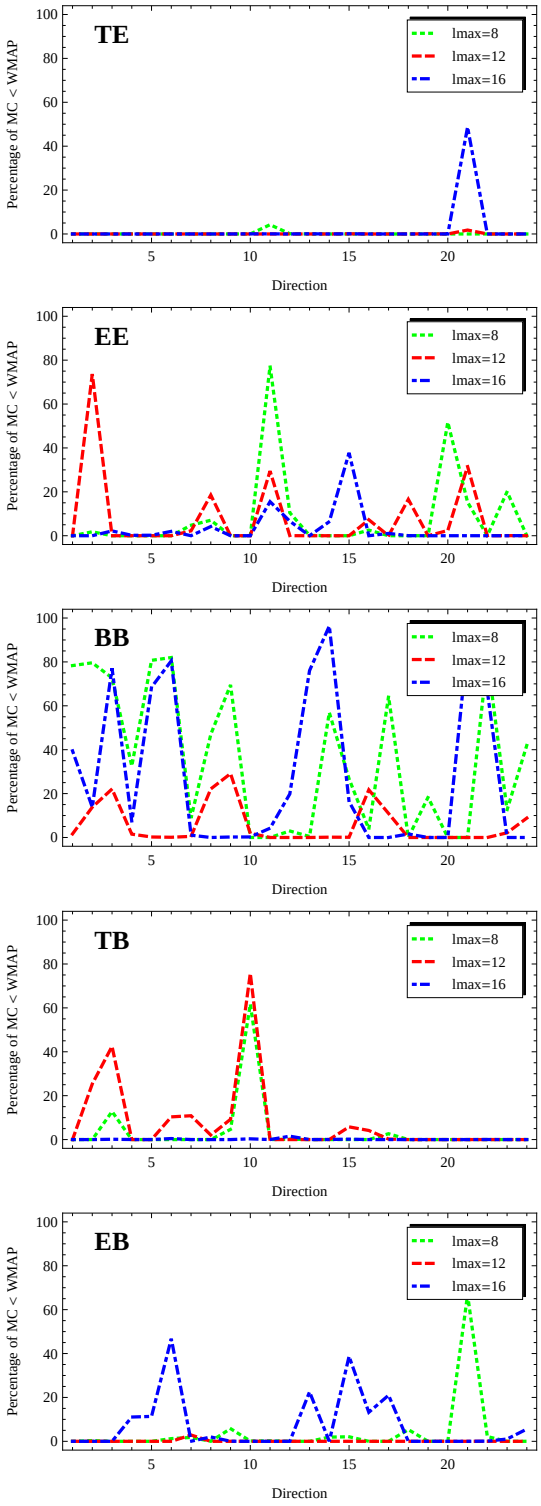

Figure 4. Percentage asymmetry of the estimator D computed for $\ell_{\rm max} = 8$ (dotted green), 12 (dashed red), 16 (dot-dashed blue) along each of the 24 directions considered. The five panels are for TE, EE, BB, TB and EB respectively.

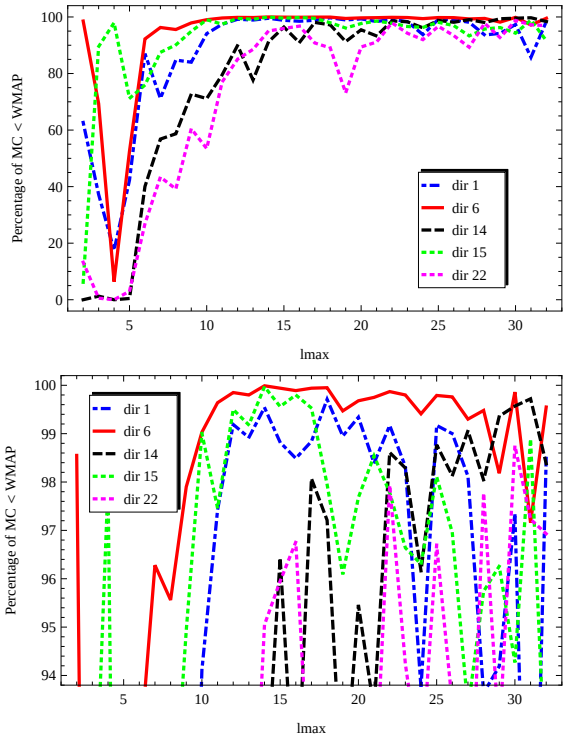

Figure 5. Percentage asymmetry of the estimator R versus $\ell_{\rm max}$. The most significative directions are shown: $\hat{n}_1$ (dot-dashed blue), $\hat{n}_6$ (solid red), $\hat{n}_{14}$ (dashed black), $\hat{n}_{15}$ (dotted green), $\hat{n}_{22}$ (dotted magenta). Bottom panel shows a zoom of the top one.

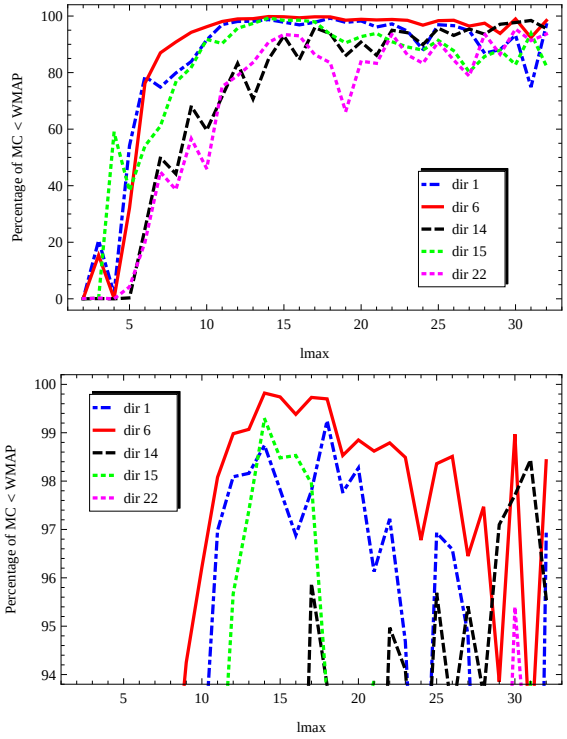

Figure 6. Same as Fig. 5 but for D.

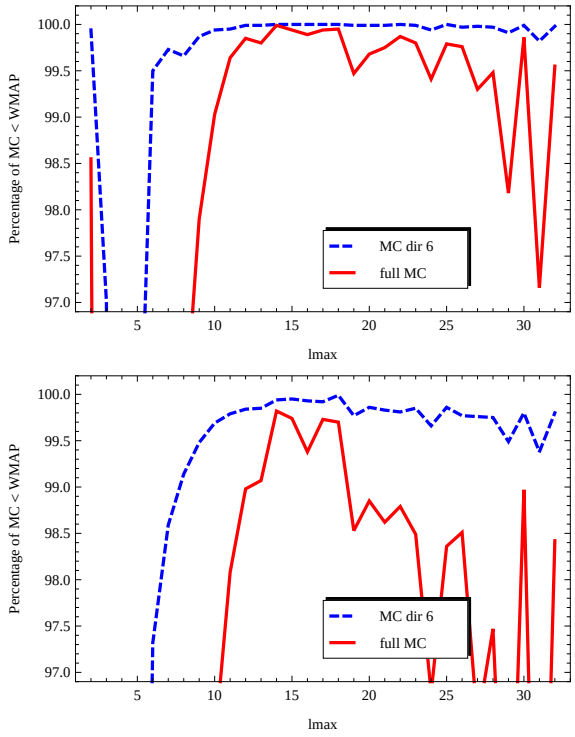

Figure 7. Comparison of the percentage asymmetry we found on WMAP data along direction $\hat{n}_6$ (solid red curve) with what one would obtain if not accounting for the 'elsewhere effect' (dashed blue curve). Top panel is for R, bottom panel for D.

maximum asymmetry for a given angular scale does not necessarily lie along the direction which maximizes the asymmetry in the data. Therefore, in order to properly sample the probability distribution from simulated skies, one has to maximize the asymmetry with respect to all the possible orientations, 24 in our analysis (see Finelli *et al.* (2011) for a similar analysis in the context of mirror symmetry). This is referred to as the 'look elsewhere' effect, and it has been properly taken into account in this work.

To stress the importance of this procedure, we show the impact on the estimated asymmetry of neglecting such effect. We fix one direction, $\hat{n}_6$, and compute R and D for 10000 CMB+noise simulated skies on the corresponding observed sky, without maximizing the estimators with respect to the other 23 directions. We compare then our distributions to WMAP asymmetry as estimated on the same sky fraction. The result of such a test is shown in Fig. 7. The dashed blue curves show the asymmetry (as a function of $\ell_{\rm max}$) for the procedure just described, whereas the solid red curves refer to the correct analysis (see also Figs. 5, 6). As expected, neglecting the 'look elsewhere effect' would lead to overestimate the significance of the asymmetry.

3.3 Global statistical significance

As pointed out by the WMAP team (Bennett *et al.* 2011), care must be taken in assessing the significance of any claimed anomaly in the data, such as the hemispherical power asymmetry. We propose here the analogous of the analysis suggested in Bennett *et al.* (2011) for the dipole

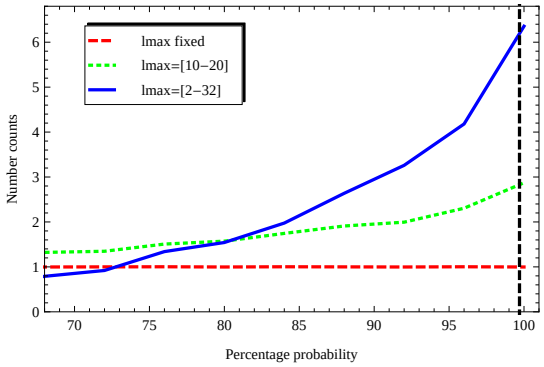

Figure 8. Distribution of the significance for η_D^{MC}. We plot the (normalized) number of simulations (y-axis) out of 10000 showing a given level of percentage asymmetry (x-axis) as computed by letting $\ell_{\rm max}$ vary for each simulation independently. Three cases are show: $\ell_{\rm max} = 14$ (red), $10 < \ell_{\rm max} < 20$ (green) and $2 < \ell_{\rm max} < 32$ (blue). The black vertical line marks the WMAP value $\eta_D^{WMAP} = 99.82\%$.

power asymmetry. The idea is to associate a probability to our estimators as obtained from the WMAP dataset without any *a posteriori* choice of the $\ell_{\rm max}$ parameter. We want to compare the maximum probability (η) of asymmetry in the data to a distribution of probabilities drawn from MC simulations where $\ell_{\rm max}$ is chosen to maximize the asymmetry for each simulation independently. We let $\ell_{\rm max}$ vary from 2 to 32. We focus on the D estimator for the temperature field. According to what shown in the previous subsection, we restrict our investigation to direction $\hat{n}_6$, for which the maximum value of D is reached for $\ell_{\rm max} = 14$ and corresponds to a significance $\eta_D^{WMAP} = 99.82\%$. Such a value has to be compared to the distribution of significance for the maximum asymmetry obtained from MC simulations (η_D^{MC}) where $\ell_{\rm max}$ is let free to move. In other words, for each extraction, $\ell_{\rm max}$ is chosen such that it maximizes the asymmetry of D.

Our results are reported in Fig. 8, where the distribution of 10000 values of η_D^{MC} is shown for three cases: $\ell_{\rm max}$ is kept fixed to a single (arbitrary) value (dashed red line), $12 < \ell_{\rm max} < 20$ (dotted green line) and $6 < \ell_{\rm max} < 32$ (solid blue line). The WMAP value is also reported as (dashed) black vertical line. As expected, we find that the probability for η_D^{WMAP} to be anomalous decreases as we widen the range allowed for $\ell_{\rm max}$. However, even for $2 < \ell_{\rm max} < 32$, the probability that a MC simulation has a value of η_D^{MC} that is larger than η_D^{WMAP} is still as low as 1.76%.

4 CONCLUSIONS

We have performed for the first time a scan of the CMB sky in temperature and polarization searching for hemispherical asymmetries at low multipoles. We have sampled the whole sky in 24 directions and computed the six angular power spectra of the CMB through our implementation of the QML estimator. As adopted in previous analysis, we have estimated the hemispherical asymmetry along each axis as the ratio and the difference of the angular power up to a given scale $\ell_{\rm max}$, which we use as free parameter in the analysis. We find the maximum hemispherical asymmetry of the temperature field if the symmetry axis is chosen along Galactic coordinates ($\theta = 132°$, $\phi = 245°$) and on angular scales $2 \leqslant \ell \leqslant 14$. The significance of such an asymmetry is 99.82% when computed through the estimator D. In order to support our findings, we have tested the impact of the *a posteriori* choice of $\ell_{\rm max}$ in the analysis. We find that the anomalous asymmetry is milder once the $\ell_{\rm max}$ parameter is released, although still as high as 98.24%. In the polarization sector, we find no significant hemispherical asymmetry, neither along the direction studied in our previous work, nor with respect to any other symmetry axis considered here.

We refer to Paci *et al.* (2010) for a forecast on PLANCK (The Planck Collaboration 2006) polarization capabilities of improving constraints on CMB hemispherical power asymmetry at large angular scales.

During the final drafting of the present work, the WMAP 9-year data and papers have been released by the collaboration [4]. We refer to future works for updates and refinements of the study presented here based on the most recent CMB data.

ACKNOWLEDGEMENTS

We acknowledge the use of the BCX and SP6 at CINECA under the agreement INAF/CINECA and the use of computing facility at NERSC. We acknowledge use of the HEALPix (Gorski *et al.* 2005) software and analysis package for deriving the results in this paper. We acknowledge the use of the Legacy Archive for Microwave Background Data Analysis (LAMBDA). Support for LAMBDA is provided by the NASA Office of Space Science. We acknowledge partial support by ASI through ASI/INAF Agreement I/072/09/0 for the PLANCK LFI Activity of Phase E2 and by MIUR through PRIN 2009.

REFERENCES

Bennett C.L. *et al.* [WMAP Collaboration] Astrophys. J. Suppl. **192** (2011) 17

Dunkley J. *et al.* [WMAP Collaboration], Astrophys. J. Suppl. **180** (2009) 306

Dvorkin C., Peiris H. V. and Hu W., Phys. Rev. D **77** (2008) 063008

Eriksen H.K., Hansen F.K., Banday A.J., Gorski K.M. and Lilje P.B., Astrophys. J. **605** (2004) 14 [Erratum-ibid. **609** (2004) 1198]

Eriksen H.K., Banday A.J., Gorski K.M., Hansen F.K. and Lilje P.B., Astrophys. J. **660** (2007) L81

F. Finelli, A. Gruppuso, F. Paci and A. A. Starobinsky, JCAP **1207** (2012) 049 [arXiv:1111.5362 [astro-ph.CO]].

Gorski K.M., Hivon E., Banday A.J., Wandelt B.D., Hansen F.K., Reinecke M. and Bartelmann M., 2005, Astrophys. J., **622**, 759-771

Gruppuso A., De Rosa A., Cabella, P., Paci F., Finelli F., Natoli P., de Gasperis G. and Mandolesi N., Mon. Not. Roy. Astron. Soc. **400** (2009) 463

[4] http://lambda.gsfc.nasa.gov/

Hansen F. K., Banday A. J. and Gorski K. M., Mon. Not. Roy. Astron. Soc. **354** (2004) 641
Hansen F. K., Banday A. J., Gorski K. M., Eriksen H. K. and Lilje P. B., Astrophys. J. **704** (2009) 1448
Hanson, D., Lewis, A. 2009, Phys. Rev. D, 80, 063004
Hoftuft J., Eriksen H. K., Banday A. J., Gorski K. M., Hansen F. K. and Lilje P. B., Astrophys. J. **699** (2009) 985
Komatsu E. *et al.* [WMAP Collaboration], Astrophys. J. Suppl. **192** (2011) 18
Y.-Z. Ma, G. Efstathiou and A. Challinor, Phys. Rev. D **83** (2011) 083005 [arXiv:1102.4961 [astro-ph.CO]].
Paci F., Gruppuso A., Finelli F., Cabella P., De Rosa A., Mandolesi N. and Natoli P., Mon. Not. Roy. Astron. Soc. **407** (2010) 399
Tegmark M., Phys. Rev. D **55**, 5895 (1997)
Tegmark M. and de Oliveira-Costa A., Phys. Rev. D **64** (2001) 063001
The Planck Collaboration, "The Scientific Programme of Planck" arXiv:astro-ph/0604069.